

# Morphologies of expansion ridges of elastic thin films onto a substrate

E. A. Jagla

*Centro Atómico Bariloche, Comisión Nacional de Energía Atómica, (8400) Bariloche, Argentina*

We consider a model of a thin film elastically attached to a rigid substrate. In the case in which the film expands relative to the substrate and assuming certain non-linear elastic behavior of the film, expansion ridges may appear, in which the material has collapsed, and the density is higher. By studying numerically this process, the possible morphologies of these collapsed regions are presented. They range from circular spots and straight stripes, to wobble polygonal patterns and ring-shaped domains. The similarity of some of these results with patterns observed in delamination of thin films and bi-phase epitaxial growth is emphasized.

PACS numbers:

## I. INTRODUCTION

When the surface of a material contracts with respect to the underlying part, tensile stresses appear in it that can lead to the formation of a crack pattern onto the surface[1]. Mud cracking can be considered to be the prototype of this surface fragmentation process. The main ingredients of surface fragmentation are a (quasi) two-dimensional film attached to a substrate (we always assume here the substrate is rigid) and a greater expansion of the substrate compared to the film as a function of some external control variable (typically humidity concentration or temperature). The film and substrate can be the same material, as in mud cracks, and in that case it is only a difference in humidity concentration or temperature what identifies film and substrate.

We will concentrate here in a process that in a certain sense is the inverse of surface fragmentation: we consider the film expanding with respect to the substrate. Due to the coupling to the substrate, the greater expansion of the film generates compressive stresses into it. No important effects are expected if the film responds linear elastically to any deformation. But if the film can collapse upon compression, a coexistence of collapsed and non-collapsed regions in the film is expected. The presentation and discussion of the different morphologies of these collapsed regions are the main aim of this paper.

The two main features that fix the morphology of collapsed regions are the degree of mismatch between film and substrate, and the kind of non-linear elastic behavior of the film, in particular, the characteristics of the collapsed state. Different possibilities are studied here. Most of the results to be presented correspond to the case in which the system is isotropic in the plane of the film (the  $x$ - $y$  plane), but some results for a model with square symmetry will also be presented. In the next Section we present the model and details on the simulation technique. In Section III we present the main results, and in Section IV we discuss two experimental situations in which the present model can be applied, namely, delamination patterns of thin film and structures appearing during bi-phase epitaxial growth. Section V contains some summary and conclusions.

## II. THE MODEL

The model to be used is an extension of that used in [2, 3] to describe fracture (see also [4] and [5]). It considers the film in a two-dimensional approximation as described by the horizontal displacement field  $\mathbf{u}(\mathbf{r})$ . From these variables the two dimensional strain tensor is calculated as  $\varepsilon_{ij} \equiv 1/2(\partial u_i/\partial x_j + \partial u_j/\partial x_i)$ . For convenience, instead of  $\varepsilon_{ij}$  we will use the following variables

$$\begin{aligned} e_1 &\equiv (\varepsilon_{11} + \varepsilon_{22})/2 \\ e_2 &\equiv (\varepsilon_{11} - \varepsilon_{22})/2 \\ e_3 &\equiv \varepsilon_{12} = \varepsilon_{21} \end{aligned} \quad (1)$$

These three variables are not independent. They satisfy the St. Venant compatibility constraint[4, 5, 6], which reads

$$(\partial_x^2 + \partial_y^2)e_1 - (\partial_x^2 - \partial_y^2)e_2 - 2\partial_x\partial_y e_3 = 0. \quad (2)$$

The free energy density of the system contains three terms: a local term  $f_0$ , a gradient term  $f_\nabla$ , and a substrate interaction term  $f_{subs}$ . The existence of a collapse transition for the film is encoded in the form of the local free energy term  $f_0$ . If we intend to describe an isotropic material, only rotationally invariant combinations of the basic variables  $e_i$  should enter the free energy. Those that can be constructed from the  $e_i$  are  $e_1$  itself, and  $e_d \equiv \sqrt{e_2^2 + e_3^2}$ . A perfectly elastic material is described by a local free energy having a quadratic minimum, namely its local free energy is of the form

$$f_0^{elastic} = B(e_1 - e_1^0)^2 + \mu(e_2^2 + e_3^2) \quad (3)$$

where  $B$  and  $\mu$  are respectively proportional to the bulk and shear modulus of the material. With the present choice, in a completely relaxed state the system has  $e_1 = e_1^0$ ,  $e_2 = e_3 = 0$ .

If the material can collapse,  $f_0$  must have some other minimum at some  $e_1^C$ ,  $e_d^C$  describing the collapsed state. The position of the collapsed minimum (in particular, the ratio  $\nu \equiv e_d^C/(e_1^C - e_1^0)$ ) will have important consequences

in the morphologies of the collapsed regions that will be observed. Different locations of the collapsed minimum will be explored and discussed here. They are qualitatively depicted in Fig. 1 as cases **A**, **B**, **C**, and **D**. In most cases the morphologies of the collapsed patterns depend only on the position of the collapsed minimum with respect to the elastic minimum, the detailed form of  $f_0$  being of minor importance. Only in case **A**, there are important variations depending on the value of the shear modulus of the collapsed state  $\mu^C$  with respect to the value in the normal phase  $\mu$ . Thus, two cases will be distinguished: **A1**, in which  $\mu^C$  is greater or equal  $\mu$ , and **A2**, in which  $\mu^C$  is lower than  $\mu$ . Note that when the collapsed state has  $e_d^C \neq 0$ , it corresponds actually to a ring of minima in the  $e_1, e_2, e_3$  space. In other words, the collapse of a circular piece of material to a state with  $e_d \neq 0$  produces an elongated object, but the orientation of this object in the  $x$ - $y$  plane can be any (in the drawings of Fig. 1 this direction was chosen as the vertical one). The explicit form of the  $f_0$  part of the free energy for the cases **A**-to-**D** is given in the appendix.

Gradient terms in the free energy will be taken in the form

$$f_{\nabla} = \sum_{i=1,2,3} \alpha_i (\nabla e_i)^2, \quad (4)$$

where  $\alpha_2 = \alpha_3$  should be chosen to retain rotational invariance. In all results below we take all  $\alpha_i \equiv \alpha$ .

The elastic interaction with the substrate is easily written in terms of the displacement variables  $\mathbf{u}$ :

$$f_{subs} = \frac{\gamma}{2} |\mathbf{u}(\mathbf{r})|^2 \quad (5)$$

where  $\gamma$  measures the stiffness of this interaction. As we take the components of  $\varepsilon$  to be our basic variables, we have to recast this energy in terms of them. This is more easily done in the Fourier space, and the result can be easily written after integration over the whole system as

$$\int d\mathbf{r}^2 f_{subs} = 2\gamma \int' d\mathbf{k}^2 \frac{|\tilde{e}_2(\mathbf{k})|^2 + |\tilde{e}_3(\mathbf{k})|^2}{k^2}, \quad (6)$$

Where  $\tilde{e}_i(\mathbf{k})$  are the Fourier transforms of the original  $e_i(\mathbf{r})$ . Here the tilde in the integral indicates that the  $k = 0$  mode is excluded. To avoid a divergent energy contribution, the value of  $\tilde{e}_1(\mathbf{k} = 0) = \bar{e}_1$  (where the bar notes a spatial average) has to be adjusted for the system to fit on average to the substrate, namely, the mismatch with the substrate is incorporated in the model precisely through the value given to  $\bar{e}_1$ .

The existence of non trivial spatial patterns in the model appears as a consequence of a competition between gradient and substrate term. In fact, in Fourier space a mode of wave vector  $\sim k$  and amplitude 1 produces a contribution to the energy of the order of  $\alpha k^2$  from the gradient terms, and  $\gamma/k^2$  from the substrate term. The sum of this two contribution has a minimum at a value of  $k$  of the order of  $(\gamma/\alpha)^{1/4}$ . This is the order of magnitude

of the main spatial variations that will be seen to appear in the simulations.

The equations of motion are taken to be of the overdamped form, namely

$$\frac{\partial e_i}{\partial t} = -\lambda \frac{\delta F}{\delta e_i} \quad (i = 1, 2, 3) \quad (7)$$

where

$$F = \int d\mathbf{r}^2 (f_0 + f_{\nabla} + f_{subs}). \quad (8)$$

The Saint Venant constraint is implemented by the use of Lagrange multipliers. Full details can be seen in [2] and [5].

### III. RESULTS

For each set of parameters, the system will settle down in a configuration that minimizes the total energy of the system. We will see that in general, metastable states appear very often in the simulations. In order to get as close as possible to the true ground state configuration, an annealing process was implemented in which a stochastic term was added to the right hand side of Eq. (7), and the intensity of this term was progressively reduced down to zero during the simulation. The final configurations obtained are good examples of the typical morphologies favored by the competition of the different energy terms.

Results will be presented for a unique set of values of the coefficients  $\alpha$  and  $\gamma$  in the gradient and substrate interaction terms [Eqs. (4) and (6)]. It can be shown that a change of these parameters can be absorbed in a rescaling of the spatial coordinate and a global redefinition of the free energy[7]. We have chosen the values  $\alpha = 3$ ,  $\gamma = 0.01$ , for which the expected spatial scale of the structures to be seen (based on the estimation in the previous section) is of the order of ten mesh parameters. Thus, the geometrical features of the patterns will be reasonably larger than the discretization of the numerical mesh, and this is appropriate to eliminate spurious effects associated to this discreteness.

The configurations obtained are presented in Figs. 2 to 6, corresponding to cases **A**-to-**D**, respectively. Each panel in each figure represents a different value of  $\bar{e}_1$ , i.e., a different degree of mismatch with the substrate. Each main plot shows the spatial distribution of  $e_1$  or  $e_d$  (depending on which is more representative in each case). The scale for this plot is indicated in the bar of the inset. The inset also shows the combined distribution of  $e_d$  vs.  $e_1$  for all elements in the system. We now discuss separately each case.

Except for the existence of the substrate, case **A** is qualitatively analogous to a well studied case, which is applicable for instance to phase separation in alloys[8, 9]. In the case in which the collapsed state has the same shear modulus than the original state (case **A1**), there

is strong evidence that the possible ground states correspond to a striped phase, a bubble phase, or a uniform phase depending on the value of  $\bar{e}_1$ . The patterns obtained in the numerical simulations presented here (Fig. 2) are in reasonable agreement with these results, although it is clear that the perfect striped phase is not easily obtained. The reason for this discrepancy is that there is a large gain in entropy when the stripes disorder, and it is very difficult numerically to get rid of this effect.

In the case in which the collapsed phase has a lower shear modulus than the original phase (case **A2**, Fig. 3), bubbles of the softer phase tend to be unstable with respect to elongation[8, 9]. This is obvious in Fig. 3 compared to Fig. 2. Note that the effect is not symmetric: if the mismatch is such that the minority phase corresponds to the more rigid phase, then the bubbles remain stable. In both cases **A1** and **A2**, for even larger mismatch (not shown) all the system becomes uniformly collapsed, with  $e_1(\mathbf{r}) = \bar{e}_1$ ,  $e_2(\mathbf{r}) = e_3(\mathbf{r}) = 0$ .

For case **B** (Fig. 4) we observe a stronger tendency to form stripes and polygonal patterns. There is also an important difference with case **A2** for large mismatch (lower-right panel): Now each element prefers to be as close as possible to the collapsed minimum, that locates at a non-zero value of  $e_d$ . However, not all elements can have the same values of  $e_2$  and  $e_3$ , since the spatial averages  $\bar{e}_2$  and  $\bar{e}_3$  should be zero. The existence of the substrate also discourages uniform phases with constant  $e_2$  or  $e_3$ . The configuration of the system is such that individual elements tend to be distributed close to the ring of minima in the  $e_2$ - $e_3$  plane. In real space, singularities appear at which  $e_2 = e_3 = 0$ , and around them the configuration point in the  $e_2$ - $e_3$  plane rotates  $2\pi$ , clockwise, or counterclockwise, thus defining ‘vortex-like’ or ‘anti-vortex-like’ defects. Density of these defects is mainly controlled by the strength of the interaction to the substrate (density tends to zero for vanishing interaction).

Cases **C** and **D** (Figs. 5 and 6) present an interesting difference in morphology with respect to previous cases: Stripes of collapsed regions present now a wavy structure. In some cases, we observe even the existence or ring shaped collapsed regions. The origin of wiggling collapsed stripes is of course dictated by the tendency of the model to minimize the energy. An elemental demonstration of the instability of straight collapsed regions with respect to wiggled patterns will be presented now. Consider the sketch of Fig. 7(a) of a straight collapsed region along the  $x$  direction. The arrows in the plot are a schematic representation of the displacement field  $\mathbf{u}(\mathbf{r})$ . Suppose that we have determined the best form of the function  $\mathbf{u}(\mathbf{r}) = u_0(y)\hat{y}$  in order to minimize the energy. We will see that in some circumstances the energy can be reduced further by changing of  $\mathbf{u}(\mathbf{r}) = u_0(y)\hat{y}$  to a new displacement field of the form  $\mathbf{u}(\mathbf{r}) = u_0(y - A \sin(kx))\hat{y}$ . Note that this represents a wiggling pattern with oscillation amplitude  $A$  and wave vector  $k$  (as sketched in Fig. 7(b)). By calculating the form of our fundamental variables  $e_1$ ,  $e_2$  and  $e_3$ , and plugging these values into

the different term of our total energy, we see that the substrate energy does not change at all. The gradient term is increased in a quantity (per unit length in the  $x$  direction) of the order of  $A^2 k^2 d$ , where  $d$  is the thickness of the collapsed region. The local term changes only because of the existence of a non-zero value of  $e_3$ . This change is also proportional to  $A^2 k^2 d$ , and the overall factor can be negative (i.e., we can have an energy gain) if  $\nu (= e_d^C / (e_1^C - e_1^0))$  is sufficiently large, as depicted in Fig. 7(c). Then we see that if this quadratic decrease of energy overcomes the quadratic increase due to the gradient terms, a wavy stripe is expected. This lowest order sketchy argument does not provide values for the amplitude  $A$  and wave vector  $k$  of the distortion. They could in principle be obtained by considering higher order terms in the expansions. We failed in doing such a calculation. We only notice that from the results of the numerical simulations (Figs. 5 and 6) it seems plausible that both  $A$  and the wave length  $k^{-1}$  are of the order of the stripe thickness  $d$ .

#### IV. PRACTICAL REALIZATIONS

We have analyzed an idealized situation of a material that has two well defined elastic configurations of minimum energy. We have shown that non-trivial morphologies may appear when a quasi-two-dimensional piece of such a material is uniformly attached to a rigid substrate. In searching for practical realizations, it will be difficult to find that all the above assumptions are satisfied, however, our model can be a good idealized case to study some practical problems. Two examples will be presented now.

The first case corresponds to the patterns observed in delamination of thin films[10]. In this case, typically, a film is grown onto a substrate, and due to chemical differences between substrate and film (which may be enhanced by temperature changes) elastic stresses develop between them. If the stresses are compressive into the film, this may induce the buckling up of part of the film, giving rise to patterns that have been termed ‘telephone-cord’ like, due to their wavy appearance. In some cases, wavy polygonal patterns of buckled regions are observed, remarkably similar to those in our Figs. 5 and 6. In delamination patterns the wave length and amplitude of the undulations observed are both of the order of the thickness of the buckled region.

This delamination process has some features that are *a priori* very different from the assumptions in our model. Two things look in fact very different: in delamination, the three dimensional nature of the process plays an important role. In contrast, our model considers a two dimensional geometry. Secondly, in delamination the interaction to the substrate is lost in the buckled regions, whereas in our model this interaction is always present. However, the similar appearance of some of our results with the delamination phenomenology is very suggestive.

We think that a justification of the similarity can be based on the following considerations: a stripe of buckled material is qualitatively depicted in Fig. 8(a). If we want to make an effective two-dimensional representation of this buckled film, we should associate to the buckled region a piece of the two dimensional model with higher density. Note also that the orientation of the buckled stripe can be any in the  $x$ - $y$  plane, but that the contraction that induces the density increase occurs only perpendicularly to the buckled ridge. This means that we can associate buckling with our collapse transition with  $\nu \simeq 1$ . In delamination, the possibility of buckling depends on the possibility of detaching from the substrate. Although in our model the interaction with the substrate is always present, the free energy with two minima takes phenomenologically into account the two configurations of the film: attached and unbuckled (represented by the isotropic minimum of our model) and detached and buckled (represented by the finite  $e_d^C$  collapsed state).

A second problem to which our model can be applied is the epitaxial growth of competing phases with different crystallographic parameters[11]. In fact, if the growing is coherent (to some extent), elastic stresses will be accumulated during growth, and which phase is chosen locally to grow the material will be dictated by a tendency to minimize the total elastic energy of the system. Thus, our model with two minima must be thought as describing the two different phases that can be chosen in the growth process. But in this case one of the previously used assumptions needs to be changed: epitaxy is strongly dependent on the crystalline structures of the phases, and isotropy of the model in the  $x$ - $y$  plane is not justified. However, the model can be easily modified to account for anisotropies in the  $x$ - $y$  plane. We will present here only a single example of the possible outcome obtained in an anisotropic model. Let us consider that the substrate has a square symmetry (assumed to be aligned with the  $x$ - $y$  coordinate axis), that one of the growing phases has also a square symmetry with a larger unit cell volume, and that the second growing phase has a rectangular symmetry with a lower unit cell volume than that of the substrate. This situation corresponds to a local free energy  $f_0$  having an elastic minimum as usual, and a collapsed minimum localized now at  $e_2 = \pm e_2^C$ ,  $e_3 = 0$ . In this way the ring of minima in the  $e_2$ - $e_3$  plane of the previous cases is replaced by a couple of minima. The exact form of  $f_0$  we use is given in the Appendix. The morphologies obtained are shown in Fig. 9. As expected, the existence of a rectangular phase reflects clearly on the morphology of the patterns. Note how upon change of the fraction of rectangular phase (which is dictated, as usual, by the degree of mismatch with the substrate), the morphology changes from stripes of rectangular phase parallel to the axis (for low density of rectangular phase), to stripes of rectangular phase along the diagonals (for the case of large fraction of rectangular phase). It is worth to be noticed that the present case can also be interpreted in the context of a model

recently introduced to describe a square-to-rectangular martensitic transformation[4, 5]. In fact, we can consider the isotropic minimum as representing the austenite phase, and the collapsed minima as the martensite phase, in its two different variants:  $e_2 = \pm e_2^C$ . In the case of Refs. [4, 5] (in which a substrate has not been included), volume change during martensitic transformation is assumed to be negligible, and a phase of diagonal stripes similar to that in the lower plots of Fig. 9 has been observed [4, 5] (note that in our case the width of the diagonal stripes is fixed by the strength of the interaction with the substrate). From the results of the first plots of Fig. 9 we can conclude that a phase of stripes along the  $x$  and  $y$  directions is favored instead when the transformation has an appreciable volume change and a finite fraction of the austenite phase remains in the system.

## V. SUMMARY AND CONCLUSIONS

Expansion ridges are analog to surface cracks, with the difference that they appear when a film expands with respect to the substrate (contrary to cracks, that appear when the film contracts with respect to the underlying material). A non-linear elastic behavior of the film, namely the possibility of a collapse upon applied stress is necessary for expansion ridges to appear. We have simulated expansion ridges through an elastic model that uses the components of the strain tensor as fundamental variables. We have shown how complex morphologies can appear due to competitive elastic interactions in the system. By changing the parameters of the model, collapsed regions in the form of bubbles, straight stripes, undulating stripes and rings have been obtained. We have argued that the model can be applied to understand the characteristics of delamination patterns in thin films, and bi-phase epitaxial growth. We have concentrated in the description of the morphologies, and then our presentation has been qualitative to a large extent. A few important things can be highlighted: The relevant spatial scale of the patterns has been seen to be fixed by a competition between interaction with the substrate and gradient effects. In the case in which the collapse is isotropic, we have qualitatively reproduced well known results in the field of alloy decomposition. Wiggle stripes of collapsed material appear when the collapse of an elemental circular piece of material is such that contraction in one direction is accompanied by expansion in the perpendicular direction. We have compared these wiggling patterns with those observed in delamination of thin films. We have also provided an example showing that anisotropy can be easily incorporated in the model, and showed that the anisotropic case may have relevance for the study of bi-phase epitaxial growth. More detailed studies and comparisons on each of these individual realizations is in progress.

## VI. APPENDIX

We give here the explicit expressions for the local free energy  $f_0$  used in each of the simulations presented in the paper. For Figs. 2 and 3, we use

$$f_0 = \left[ \frac{e_d^2}{2} + (e_1 - 1)^2 \right] [1 + \tanh(3e_1)] + \left[ C_1 \frac{e_d^2}{2} + (e_1 + 1)^2 \right] [1 - \tanh(-3e_1)] \quad (9)$$

with  $C_1 = 1$  in Fig. 2, and  $C_1 = 0$  in Fig. 3. In Figs. 4, 5, 6, we use

$$f_0 = \left[ \frac{e_d^2}{2} + \frac{e_d^4}{4} + (e_1 - C_3)^2 \right] [1 + \tanh(C_2 e_1)] + \left[ -\frac{e_d^2}{2} + \frac{e_d^4}{4} + (e_1 + C_3)^2 + \frac{1}{4} \right] [1 - \tanh(-C_2 e_1)] \quad (10)$$

with  $C_2 = 2$  and  $C_3 = 0.4$  in Fig. 4;  $C_2 = 3.5$  and  $C_3 = 0.2$  in Fig. 5; and  $C_2 = 4$  and  $C_3 = 0.1$  in Fig. 6. Finally, in Fig. 9 we use

$$f_0 = \left[ \frac{e_2^2}{2} + \frac{e_2^4}{4} + (e_1 - C_3)^2 \right] [1 + \tanh(C_2 e_1)] + \left[ -\frac{e_2^2}{2} + \frac{e_2^4}{4} + (e_1 + C_3)^2 + \frac{1}{4} \right] [1 - \tanh(-C_2 e_1)] + e_3^2 \quad (11)$$

with  $C_2 = 2$  and  $C_3 = 0.4$ .

- 
- [1] K. Leung and J. V. Andersen, *Europhys. Lett.* **38**, 589 (1997); S. Kitsunozaki, *Phys. Rev. E*, **60**, 6449 (1999); A. Groisman and E. Kaplan, *Europhys. Lett.* **25**, 415 (1994); P. Meakin, *Science* **252**, 226 (1991); W. Korneta, S. K. Mendiratta, and J. Menteiro, *Phys. Rev. E* **57**, 3142 (1998); K. A. Shorlin, J. R. de Bruyn, M. Graham, and S. W. Morris, *Phys. Rev. E* **61**, 6950 (2000); T. Hornig, I. M. Sokolov, and A. Blumen, *Phys. Rev. E* **54**, 4293 (1996); K. Leung and Z. Neda, *Phys. Rev. Lett.* **85**, 662 (2000).
- [2] V. I. Marconi and E. A. Jagla, *Phys. Rev. E* **71**, 036110 (2005).
- [3] E. A. Jagla, *Phys. Rev. E* **69**, 056212 (2004).
- [4] S. Kartha, J. A. Krumhansl, J. P. Sethna, and L. K. Wickham, *Phys. Rev. B* **52**, 803 (1995).
- [5] S. R. Shenoy, T. Lookman, A. Saxena, and A. R. Bishop, *Phys. Rev. B* **60**, R12537 (1999); T. Lookman, S. R. Shenoy, K. O. Rasmussen, A. Saxena, and A. R. Bishop, *Phys. Rev. B* **67**, 024114 (2003).
- [6] D. Chandrasekharaiah and L. Debnath, *Continuum Mechanics* (Academic Press, San Diego, 1994).
- [7] E. A. Jagla, *Phys. Rev. E* **70**, 046204 (2004).
- [8] C. Sagui and R. C. Desai, *Phys. Rev. Lett.* **71**, 3995 (1993); *Phys. Rev. E* **49**, 2225 (1994); *Phys. Rev. E* **52**, 2807 (1995); D. Orlikowski, C. Sagui, A. Somoza, and C. Roland, *Phys. Rev. B* **59**, 8646 (1999).
- [9] A. Onuki, *Phase Transition Dynamics* (Cambridge University Press, Cambridge, 2002).
- [10] J. Colin, F. Cleymand, C. Coupeau, and J. Grilhé, *Phil. Mag. A* **80**, 2559 (2000); F. Cleymand, C. Coupeau, and J. Grilhé, *Scripta Mat.* **44**, 2623 (2001); C. Coupeau, *Thin Solid Films* **406**, 190 (2002); M. -W. Moon, H. M. Jensen, J. W. Hutchinson, K. H. Oh, and A. G. Evans, *J. Mech. Phys. Sol.* **50**, 2355 (2002); M. -W. Moon, K. -R. Lee, K. H. Oh, and J. W. Hutchinson, *Acta Mater.* **52**, 3151 (2004).
- [11] H. Zheng, J. Wang, S. E. Lofland, Z. Ma, L. Mohaddes-Ardabili, T. Zhao, L. Salamanca-Riba, S. R. Shinde, S. B. Ogale, F. Bai, D. Viehland, Y. Jia, D. G. Schlom, M. Wuttig, A. Roytburd, and R. Ramesh, *Science* **303**, 661 (2004); J. Li, I. Levin, J. Slutsker, V. Provenzano, P. K. Schenck, R. Ramesh, J. Ouyang, and A. L. Roytburd, *Appl. Phys. Lett.* **87**, 072909 (2005); A. Artemev, J. Slutsker, and A. L. Roytburd, *Acta Mater.* **53**, 3425 (2005).

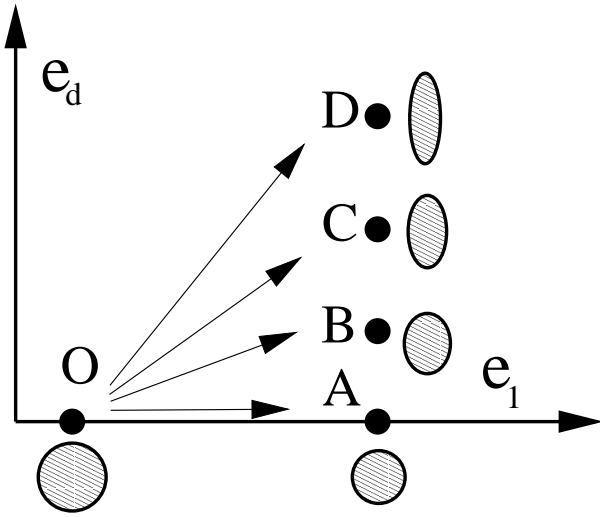


FIG. 1: Different possibilities for the location of the collapsed minimum in the  $e_1$ - $e_d$  plane. The elastic minimum is located at  $O$ . The sketches show qualitative an originally circular piece of material at  $O$  and its collapsed form for different locations of the collapsed minimum. In cases **A** and **B** the an original circular piece of material contracts in all directions, whereas for **C** and **D** there is a direction in which it actually expands (chosen here to be the vertical direction).

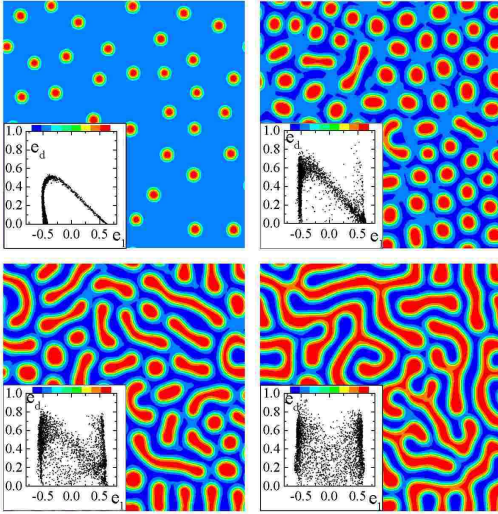


FIG. 2: (Color online) Spatial configurations obtained for case **A1**, for values of  $\bar{e}_1$  equal to  $-0.4$ ,  $-0.2$ ,  $-0.1$ , and  $0.2$  (from left to right and from top to bottom). The shadows indicate values of  $e_1$ , with the scale indicated in the inset. In the inset plots, the distribution of  $e_d$  vs.  $e_1$  is shown for all elements of the system.

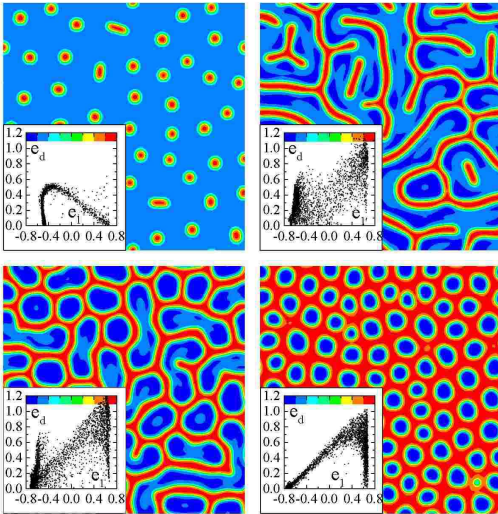


FIG. 3: (Color online) Same as Fig. 2 for case **A2**, and values of  $\bar{e}_1$  of  $-0.4$ ,  $-0.2$ ,  $-0.1$ , and  $0$ .

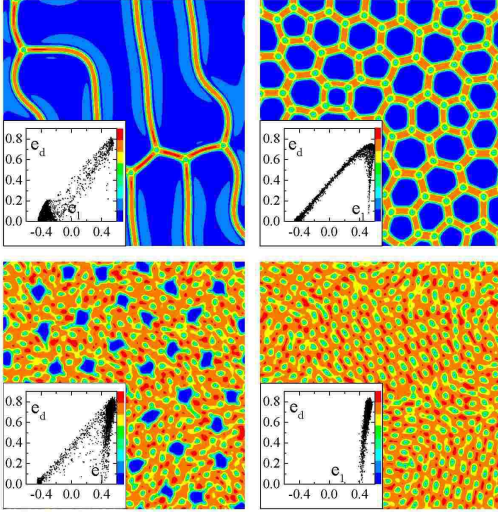


FIG. 4: (Color online) Same as Fig. 2 for case **B**, and values of  $\bar{e}_1$  of  $-0.2, 0, 0.4$ , and  $0.5$  (note that in this and next two Figures, the main plot shows values of  $e_d$ , instead of  $e_1$ ).

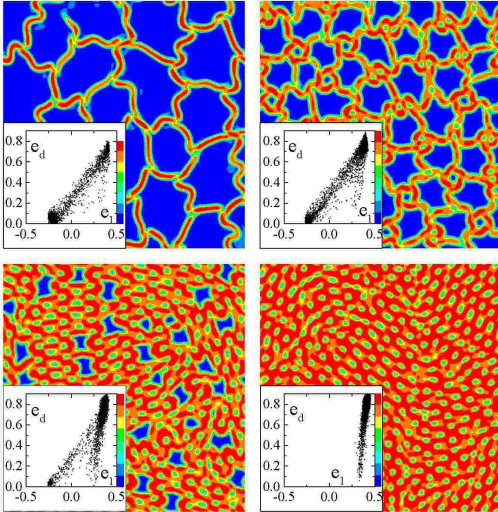


FIG. 5: (Color online) Same as Fig. 4 for case **C**, and values of  $\bar{e}_1$  of  $-0.05, 0.1, 0.3$ , and  $0.4$ .



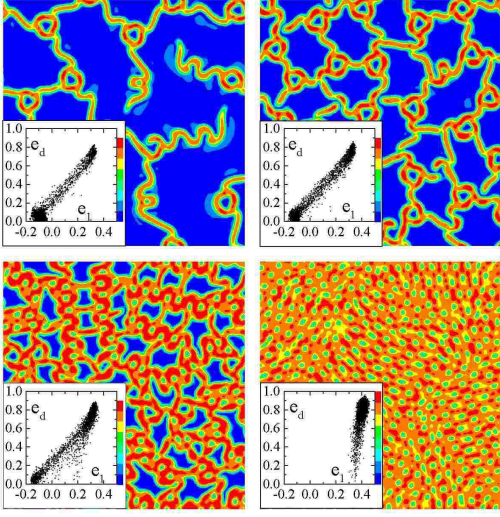


FIG. 6: (Color online) Same as Fig. 4 for case **D**, and values of  $\bar{e}_1$  of  $-0.005$ ,  $0.05$ ,  $0.2$ , and  $0.4$ .

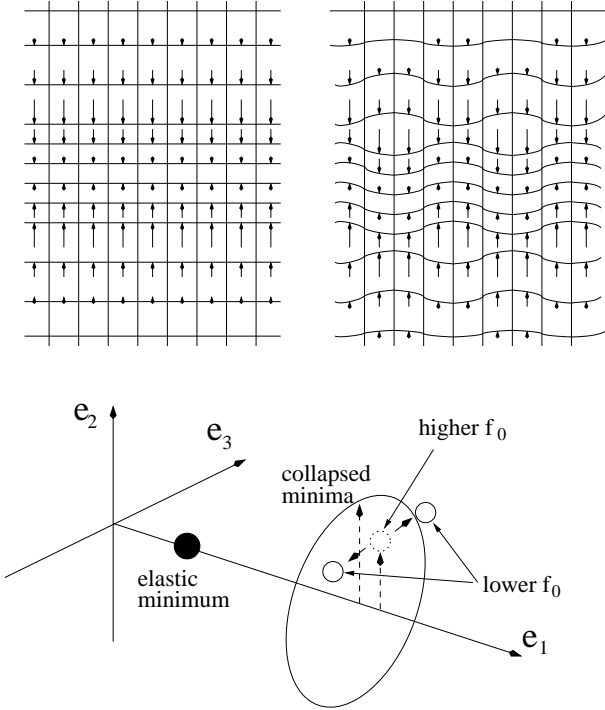


FIG. 7: (a) The structure of a straight collapsed region. Arrows indicate qualitatively the displacement  $\mathbf{u}(\mathbf{r})$ . This configuration can be unstable with respect to the deformation shown in (b), for certain forms of the local free energy  $f_0$ . In fact, part (c) illustrates how a piece of material collapsed in a single direction (represented by the dotted circle) can lower its energy by generating a finite shear distortion  $e_3$  if this brings it closer to the ring of minima of the potential.

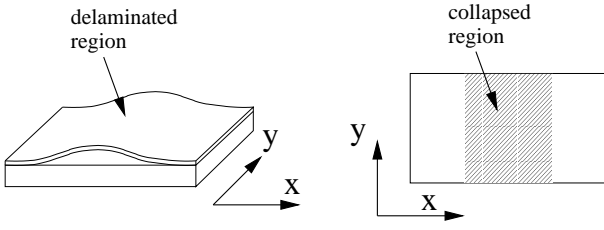


FIG. 8: A stripe of delaminated thin film, and the qualitative equivalent as a region of collapsed material in our model.

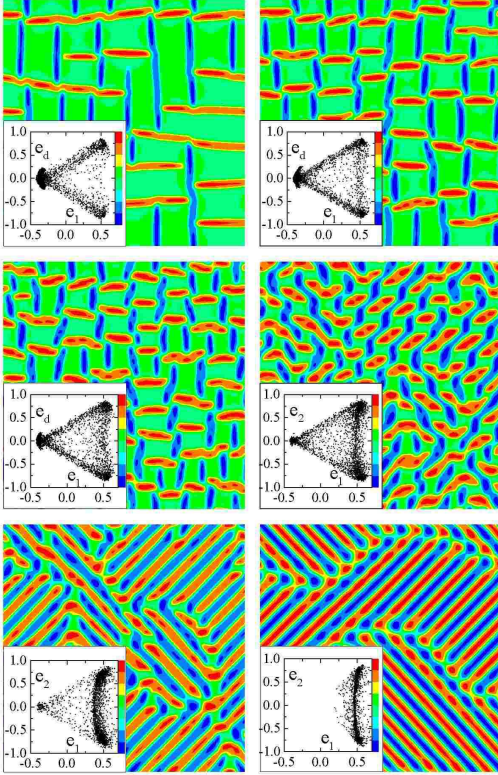


FIG. 9: (Color online) Morphologies for an anisotropic case in which the collapsed minima are located at  $e_2 = \pm e_2^C$ ,  $e_3 = 0$ . The values of  $\bar{e}_1$  for the plots are  $-0.1, 0, 0.1, 0.3, 0.4$ , and  $0.5$  respectively. Note that as long as there is some fraction of the system in the isotropic elastic minimum (first three plots) the morphology of the collapsed regions is that of inter-crossed stripes along  $x$  and  $y$ , while when the fraction of the system in the elastic configuration is negligible (last two plots) the morphology changes to stripes along the diagonals.